Controlled hydroxy-fluorination reaction of anatase to promote Mg 2+ mobility in rechargeable magnesium batteries

Jiwei Ma, Toshinari Koketsu, Benjamin J Morgan, Christophe Legein, Monique Body, Peter Strasser, Damien Dambournet

Controlled Hydroxy-Fluorination Reaction of Anatase to Promote Mg²⁺ Mobility in Rechargeable Magnesium Batteries

Jiwei Ma,[a,b,†] Toshinari Koketsu,[c,†] Benjamin. J. Morgan,[d, e] Christophe Legein,[f] Monique Body,[f] Peter Strasser[c] and Damien Dambournet*[a,g]

In anatase TiO₂, substituting oxide anions with singly charged (F,OH) anions allows the controlled formation of cation vacancies, which act as reversible intercalation sites for Mg²⁺. We show that ion-transport (diffusion coefficients) and intercalation (reversible capacity) properties are controlled by two critical parameters: the vacancy concentration and the local anionic environnment. Our results emphasise the complexity of this behaviour, and highlight the potential benefits of chemically controlling cationic-defects in electrode materials for rechargeable multivalent-ion batteries.

Fluorination of inorganic frameworks has been widely used as a strategy for tuning their material properties through the modulation of composition and structure.[1–4] Solution-based methods, which rely on reactive molecular precursors, are effective in controlling the degree of fluorination of solids. Using a derived sol-gel chemistry, Kemnitz *et al*.[5] first proposed the synthesis of a metal fluoride through reaction of metal alkoxide with anhydrous hydrofluoric acid (HF). This reaction M-OR + HF → M-F + R-OH, was named fluorolysis, by analogy to hydrolysis.[6] The similar nucleophilic characters of HF and H₂O indicates similar reactivities, with partial charges $\delta(F) = -0.42$ and $\delta(O) = -0.40$.[7] This allows targeted combined use of H₂O and HF to tune the compositional and structural features of solids prepared from metal alkoxide. We have recently investigated the reaction of titanium alkoxide with aqueous HF, and exploiting this chemistry to tune both composition and structure.[8–11] The composition of anatase TiO₂ can be modified according to the general chemical formula $Ti_{1-x-y}\square_{x+y}O_{2-4(x+y)}F_{4x}(OH)_{4y}$, where $\square$ represents a titanium vacancy. Concomitant hydrolysis and fluorolysis reactions cause F⁻ and OH⁻ anions to substitute O²⁻, accompanied by the formation of charge-compensating titanium vacancies. These cationic vacancies promote reversible electrochemical insertion of Mg²⁺ and Al³⁺ ions, making this synthetic approach a possible route to developing electrode materials for multivalent-ion batteries.[12]

Rechargeable Mg batteries have been suggested as candidates for "beyond lithium-ion" electrochemical storage.[13] Aurbach *et al*.[14] first demonstrated reversible Mg²⁺ intercalation in host frameworks based on the Chevrel structure, Mo_6Ch_8 (*Ch* = S, Se). Subsequent research on multivalent electrodes has shown that Mg²⁺ intercalation chemistry often differs from that of Li⁺. Divalent Mg²⁺ cations experience strong electrostatic interactions with oxide lattices, which inhibits Mg²⁺ mobility.[15–19] Previous suggestions to address this issue include using hosts with "soft" polarisable anions,[20,21] operating at elevated temperatures,[22] and identifying host frameworks with low diffusion migration barriers.[17,23–25] Within this context, oxides have been predicted to offer high volumetric energy densities, based on their higher typical crystal densities.[26]

Our approach to enhancing Mg²⁺ diffusion in anatase TiO₂ is to chemically introduce high concentrations of cation vacancies. This has three consequences: (i) cationic vacancies act as selective host sites for Mg²⁺; (ii) at high concentration, vacancies are randomly distributed at the particle level (as revealed by TEM data[12]) providing a continuous disordered network of vacant sites which supports facile diffusion of Mg²⁺; (iii) monovalent F⁻ and OH⁻ anions preferentially occupy sites adjacent to titanium vacancies, indicated by ¹⁹F NMR and DFT data[8,12,27]. This reduces the net electrostatic interactions between intercalated Mg²⁺ ions and the host, relative to the stoichiometric parent oxide.[12]

a. Sorbonne Université, CNRS, Physico-chimie des électrolytes et nano-systèmes interfaciaux, PHENIX, F-75005 Paris, France.
Email: damien.dambournet@sorbonne-universite.fr

b. Institute of New Energy for Vehicles, School of Materials Science and Engineering, Tongji University, Shanghai 201804, China.

c. The Electrochemical Energy, Catalysis, and Materials Science Laboratory, Department of Chemistry, Technical University Berlin, 10623 Berlin, Germany.

d. Department of Chemistry, University of Bath, BA2 7AY Bath, United Kingdom.

e. The Faraday Institution, Quad One, Harwell Science and Innovation Campus, Didcot, UK

f. Institut des Molécules et Matériaux du Mans (IMMM) - UMR 6283 CNRS, Le Mans Université, Avenue Olivier Messiaen, 72085 Le Mans, Cedex 9, France

g. Réseau sur le Stockage Electrochimique de l'Energie (RS2E), FR CNRS 3459, 80039 Amiens, France

† These authors contributed equally to the work.

† Electronic Supplementary Information (ESI) available: Details of synthesis, GITT, NMR, proportions of anionic environments in the vicinity of the vacancy, DFT calculations. See DOI: 10.1039/x0xx00000x

Here, we report how tuning the chemical composition of $Ti_{1-x-y}\Box_{x+y}O_{2-4(x+y)}F_{4x}(OH)_{4y}$ modifies Mg^{2+} intercalation and transport properties. We find that the presence of titanium vacancies enabled reversible Mg^{2+} intercalation, and that the local anionic environment modifies the intercalation behaviour. Our work provides a new strategy to promote Mg^{2+} intercalation that can serve as a platform in understanding critical local structural features favouring Mg^{2+} mobility.

We consider the reaction of titanium alkoxide and aqueous HF solution treated at mild temperature to control the composition of $Ti_{1-x-y}\Box_{x+y}O_{2-4(x+y)}F_{4x}(OH)_{4y}$ electrode materials. Two temperatures were selected: 90 °C and 130 °C (see the ESI† for details). ^{19}F NMR was used to determine the fluorine content, the vacancy concentration was quantified by structural analysis of the PDF data and the OH content was deduced from charge neutrality. Increasing the synthesis temperature causes the vacancy concentration to decrease, mostly due to a deshydroxylation of the framework. The determined chemical compositions were $Ti_{0.78}\Box_{0.22}O_{1.12}F_{0.40}(OH)_{0.48}$ (90 °C) and $Ti_{0.87}\Box_{0.13}O_{1.48}F_{0.36}(OH)_{0.16}$ (130 °C).[28]

The electrochemical activity of $Ti_{1-x-y}\Box_{x+y}O_{2-4(x+y)}F_{4x}(OH)_{4y}$ samples *vs*. Mg^{2+}/Mg was assessed using a three-electrode Swagelok cell with Mg metal as counter and reference electrodes and phenyl-magnesium-chloride (PhMgCl) and $AlCl_3$ (molar ratio 2:1) complex in tetrahydrofuran solution as the electrolyte (see ESI†). **Figure 1a** shows galvanostatic discharge/charge curves obtained for the first three cycles at 20 mA g^{-1}.

We observe that the reversible capacity for Mg intercalation increases with the concentration of vacancies. Both compositions exhibit capacities greater than 110 mAh g^{-1} after the third cycles, which is significantly higher than that of the defect-free TiO_2, which has a reversible capacity of around 30 mAh g^{-1}, underlining the beneficial impact of vacancies. The theoretical capacities assuming Mg^{2+} intercalation only in vacancies are 166 mAh g^{-1} for $Ti_{0.78}\Box_{0.22}O_{1.12}F_{0.40}(OH)_{0.48}$ and 95 mAh g^{-1} for $Ti_{0.87}\Box_{0.13}O_{1.48}F_{0.36}(OH)_{0.16}$. For the latter compound, the observation of a capacity larger than the theoretical value suggests an additional contribution from insertion at native interstitial sites. Long term cycling **(Figure 1b)** at a high rate of 200 mA g^{-1} shows that the samples can sustain capacities above 70 mAh g^{-1} after 100 cycles, specifically 85 mAh g^{-1} (0.112 Mg^{2+}) for $Ti_{0.78}\Box_{0.22}O_{1.12}F_{0.40}(OH)_{0.48}$ and 72 mAh g^{-1} (0.098 Mg^{2+}) for $Ti_{0.87}\Box_{0.13}O_{1.48}F_{0.36}(OH)_{0.16}$. The material with the highest vacancy concentration displays the highest capacity under low current densities **(Figure 1c)**. At higher cycling rates, however, this trend is less pronounced, with the reversible capacity less strongly correlated with Ti vacancy concentration, which might indicate an increased pseudo-capacitance effect.

To gain insight into the Mg^{2+} intercalation kinetics, we performed galvanostatic intermittent titration (GITT) experiments (see ESI† for details). In both samples, the relaxation period to equilibrium, characterized by a voltage increase, sensitively depends on the inserted Mg^{2+} concentration. Moreover, in near-equilibrium condition, the number of intercalated Mg^{2+} exceeds the concentration of vacancies, again suggesting the contribution of interstitial sites

to the intercalation capacity. To better probe the vacancy concentration dependence of the Mg^{2+} transport properties, we plotted the variation in Mg^{2+} diffusion coefficients (see ESI† for details) during the first discharge **(Figure 2)**. In both samples, the diffusion coefficient decreases with progressive Mg^{2+} intercalation, which can be attributed to mutual blocking by Mg^{2+} ions, and increased correlation effects that decrease the macroscopic diffusion coefficient.[12,29,30] This "blocking" effect is less pronounced for the sample containing the highest concentration of vacancies, indicating a reduced interaction between intercalated Mg^{2+} ions.
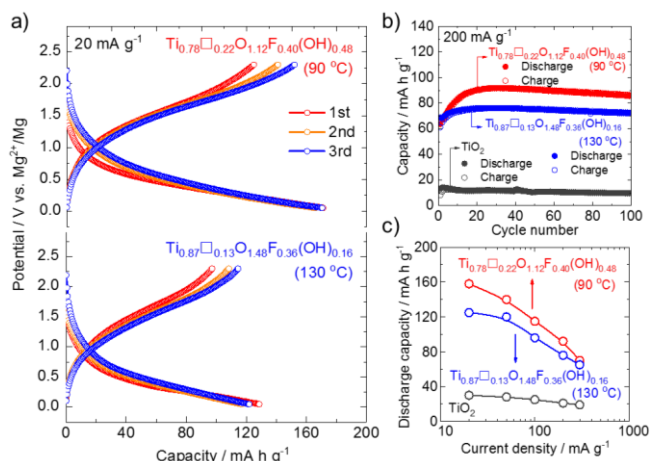

Fig 1. a) Galvanostatic first three discharge–charge curves for $Ti_{0.78}\Box_{0.22}O_{1.12}F_{0.40}(OH)_{0.48}$ (90 °C) and $Ti_{0.87}\Box_{0.13}O_{1.48}F_{0.36}(OH)_{0.16}$ (130 °C) electrodes *vs.* Mg^{2+}/Mg. Cells were cycled under 20 mA g^{-1} in the potential range 0.05–2.3 V. b) Long term cycling under 200 mA g^{-1}. c) Rate capability. For comparison purpose, the data obtained for pure anatase TiO_2 were included.
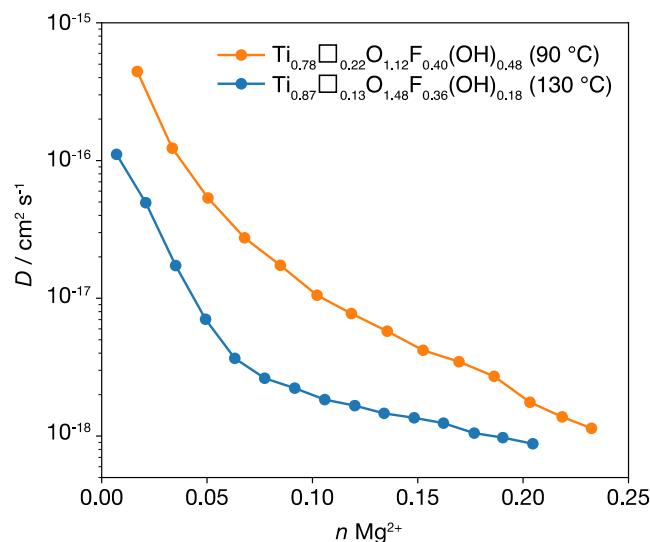

Fig 2. Variation of the diffusion coefficient of Mg^{2+} (determined using the GITT experiments) as a function of its concentration.

Moreover, we previously emphasized the occurrence of two domains observed during the variation of the Mg^{2+} diffusion coefficient in $Ti_{0.78}\square_{0.22}O_{1.12}F_{0.40}(OH)_{0.48}$.[12] This feature is more pronounced in $Ti_{0.87}\square_{0.13}O_{1.48}F_{0.36}(OH)_{0.16}$. In anatase $Ti_{1-x-y}\square_{x+y}O_{2-4(x+y)}F_{4x}(OH)_{4y}$, vacancies can either be isolated (single vacancies) or adjacent (paired vacancies). As shown by previous DFT calculations[12] and ^{19}F solid state NMR (see ESI†), upon discharge, Mg^{2+} is inserted preferentially at paired vacancies (effectively converting these to single-vacancies) and is subsequently inserted at single-vacancies. Considering the relative proportions of single vacancy and di-vacancies that are 39% and 13% for $Ti_{0.78}\square_{0.22}O_{1.12}F_{0.40}(OH)_{0.48}$ and 29% and 5% for $Ti_{0.87}\square_{0.13}O_{1.48}F_{0.36}(OH)_{0.16}$, the number of Mg^{2+} that can be accommodate by one of the vacant site in the di-vacancy is 0.045 for $Ti_{0.78}\square_{0.22}O_{1.12}F_{0.40}(OH)_{0.48}$ and 0.016 for $Ti_{0.87}\square_{0.13}O_{1.48}F_{0.36}(OH)_{0.16}$. These numbers are consistent with a stronger blocking effect occurring at lower vacancy numbers. The local anionic environment around the vacancy is also an important parameter that affects intercalation properties.[28,31] To illustrate this, we have considered the ratios of local anionic environments for a vacancy, $\square X_6$, with X = F, O(OH), for $Ti_{0.78}\square_{0.22}O_{1.12}F_{0.40}(OH)_{0.48}$ and $Ti_{0.87}\square_{0.13}O_{1.48}F_{0.36}(OH)_{0.16}$, assuming a random distribution of anions around each vacancy (**Figure 3a**; see the ESI† for details). This statistical model predicts that the local anionic environment of Mg^{2+} is, on average, more fluorinated in $Ti_{0.87}\square_{0.13}O_{1.48}F_{0.36}(OH)_{0.16}$. Individual vacancies, however, can have varied local anion environments, from fully fluorinated, to hydroxyfluorinated to fully hydroxylated.

To quantify the effect of this variation in anionic environment, we have performed DFT calculations of Mg intercalation energies (relative to metallic Mg) in the single vacancy system $Ti_{127}\square_1O_{252}X_4$, where the vacancy is surrounded by 2O and $4X$ with X = F and/or OH. We have considered 5 configurations, varying from fully fluorinated (4F; **Figure 3c**) to hydroxyfluorinated (3F + 1OH, 2F + 2OH, 1F + 3OH) to hydroxylated (4OH; **Figure 3d**) (details given in the ESI†) **(Figure 3b; blue points)**. For all five anion environments, Mg^{2+} intercalation is significantly more energetically favourable than intercalation into stoichiometric anatase TiO_2. We find that Mg^{2+} intercalation is most favourable at fully fluorinated cation vacancies, and that replacing F with OH groups makes intercalation less energetically favourable. We observe no clear energetic trend as OH progressively replaces F, which we attribute to the geometric complexity for OH-containing systems in accommodating Mg^{2+} while also optimising internal hydrogen bonding between OH groups and lattice oxide ions. In general, however, we obtain the consistent result that partially- or fully-hydroxylated anatase TiO_2 is predicted to readily intercalate Mg^{2+} ions, in agreement with our experimental results discussed above.

Our discharge/charge data and diffusion data (above) both indicate an Mg^{2+} intercalation capacity that exceeds the number of cation vacancies, suggesting a contribution from interstitial sites. To better understand how the presence of $V_{Ti}+4X_O$ complexes affects the intercalation properties of neighbouring interstitial sites, we performed additional DFT calculations of
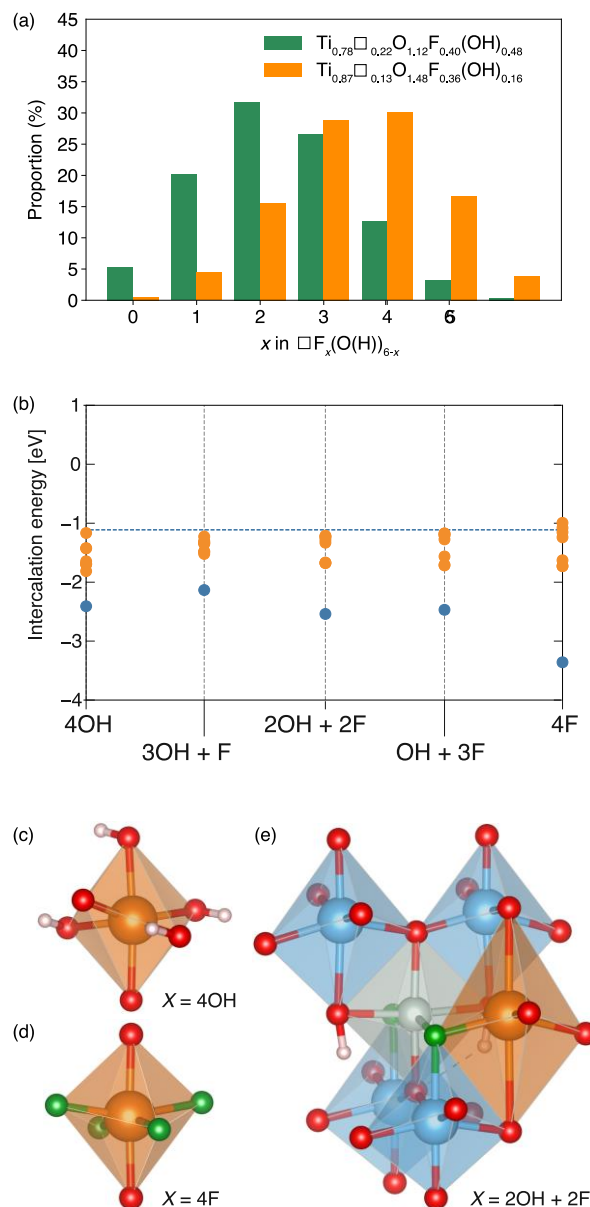
Fig 3. (a) Proportions of anionic environments in the vicinity of the vacancy, *i.e.*, $\square X_6$ with X = F, O(OH), assuming a random distribution of the anions around the vacancy. (b) Intercalation energy of Mg^{2+} in a $Ti_{127}\square_1O_{252}X_4$ supercell for X = {F, OH}. The horizontal dashed line shows the intercalation energy for Mg^{2+} in stoichiometric anatase TiO_2. (c) Optimised structure of Mg (orange) occupying V_{Ti} with 4 adjacent X = OH anions. (d) Optimised structure of Mg occupying V_{Ti} with 4 adjacent X= F anions. (e) Optimised structure of V_{Ti} (grey) + 2OH + 2F with Mg occupying an adjacent interstitial site. Source: the data set and code to generate panel (b) and the figure file, are available under the CC-BY licence as part of Ref. 27.

Mg intercalation at sets of eight adjacent interstitial sites, for each anion combination. **(Figure 3b, orange points; also Figure 3e)**. For all anion configurations, we find a spread of intercalation energies that depend on the specific arrangement of anions and the Mg interstitial position relative to the cation vacancy. In all cases we predict intercalation energies that are more favourable than intercalation at interstitial sites in

stoichiometric anatase TiO_2. We hypothesise that this effect is partially due to the adjacent cation vacancy allowing the lattice strain produced by Mg insertion to be more readily accommodated than in pristine TiO_2, and provides an explanation for the surplus intercalation capacity relative to the formal cation vacancy number we observe in experiment.

Summary. We have investigated the effect of anion chemistry and vacancy concentration on electrochemical Mg^{2+} insertion in (F,OH)-substituted anatase TiO_2. We have found that the concentration of vacancies strongly influences the transport properties of Mg^{2+}, and the combination of substituting (F,OH) anions affects the local intercalation environment experienced by the Mg^{2+} ions. This neighbouring anion effect causes variations in intercalation voltage of up to 0.5 eV, with fully fluorinated environments giving higher intercalation potentials. The formation of $V_{Ti}+4(F,OH)_O$ defects not only provides V_{Ti} sites that accommodate Mg insertion, but also makes Mg insertion more favourable at neighbouring interstitial sites, giving a net Mg intercalation capacity greater than the number from pure Ti vacancy occupation. Our findings provide new evidence and understanding about the critical role of the local chemical environment at intercalation sites on Mg^{2+} insertion.

Conflicts of interest

There are no conflicts to declare.

Notes and references

Data Access Statement. The DFT dataset supporting this study is available from the University of Bath Research Data Archive (awaiting doi)[27], published under the CC-BY-40 license. This dataset contains all input parameters and output files for the DFT calculations, scripts for collating the data used in our analysis, and code to generate Fig. 3b.

1   E. Kemnitz and D.-H. Menz, *Prog. Solid State Chem.*, 1998, **26**, 97–153.

2   A. Demourgues, N. Penin, D. Dambournet, R. Clarenc, A. Tressaud and E. Durand, *J. Fluor. Chem.*, 2012, **134**, 35–43.

3   M. Leblanc, V. Maisonneuve and A. Tressaud, *Chem. Rev.*, 2015, **115**, 1191–1254.

4   N. Pereira, F. Badway, M. Wartelsky, S. Gunn and G. G. Amatucci, *J. Electrochem. Soc.*, 2009, **156**, A407–A416.

5   E. Kemnitz, U. Groß, S. Rüdiger and C. S. Shekar, *Angew. Chem. Int. Ed.*, 2003, **42**, 4251–4254.

6   S. Rüdiger and E. Kemnitz, *Dalton Trans.*, 2008, 1117–1127.

7   J. Livage, M. Henry and C. Sanchez, *Prog. Solid State Chem.*, 1988, **18**, 259–341.

8   W. Li, D. Corradini, M. Body, C. Legein, M. Salanne, J. Ma, K. W. Chapman, P. J. Chupas, A.-L. Rollet, C. Julien, K. Zhagib, M. Duttine, A. Demourgues, H. Groult and D. Dambournet, *Chem. Mater.*, 2015, **27**, 5014–5019.

9   W. Li, M. Body, C. Legein, O. J. Borkiewicz and D. Dambournet, *Inorg. Chem.*, 2016, **55**, 7182–7187.

10 W. Li, M. Body, C. Legein and D. Dambournet, *Cryst. Growth Des.*, 2016, **16**, 5441–5447.

11 W. Li, M. Body, C. Legein, O. J. Borkiewicz and D. Dambournet, *Eur. J. Inorg. Chem.*, 2017, **2017**, 192–197.

12 T. Koketsu, J. Ma, B. J. Morgan, M. Body, C. Legein, W. Dachraoui, M. Giannini, A. Demortière, M. Salanne, F. Dardoize, H. Groult, O. J. Borkiewicz, K. W. Chapman, P. Strasser and D. Dambournet, *Nat. Mater.*, 2017, **16**, 1142.

13 J. W. Choi and D. Aurbach, *Nat. Rev. Mater.*, 2016, **1**, 16013.

14 D. Aurbach, Z. Lu, A. Schechter, Y. Gofer, H. Gizbar, R. Turgeman, Y. Cohen, M. Moshkovich and E. Levi, *Nature*, 2000, **407**, 724–727.

15 G. G. Amatucci, F. Badway, A. Singhal, B. Beaudoin, G. Skandan, T. Bowmer, I. Plitz, N. Pereira, T. Chapman and R. Jaworski, *J. Electrochem. Soc.*, 2001, **148**, A940–A950.

16 E. Levi, M. D. Levi, O. Chasid and D. Aurbach, *J. Electroceramics*, 2009, **22**, 13–19.

17 M. Liu, Z. Rong, R. Malik, P. Canepa, A. Jain, G. Ceder and K. A. Persson, *Energy Environ. Sci.*, 2015, **8**, 964–974.

18 G. S. Gautam, P. Canepa, R. Malik, M. Liu, K. Persson and G. Ceder, *Chem. Commun.*, 2015, **51**, 13619–13622.

19 S.-H. Bo, C. P. Grey and P. G. Khalifah, *Chem. Mater.*, 2015, **27**, 4630–4639.

20 X. Sun, P. Bonnick and L. F. Nazar, *ACS Energy Lett.*, 2016, **1**, 297–301.

21 X. Sun, P. Bonnick, V. Duffort, M. Liu, Z. Rong, K. A. Persson, G. Ceder and L. F. Nazar, *Energy Environ. Sci.*, 2016, **9**, 2273–2277.

22 V. Duffort, X. Sun and L. F. Nazar, *Chem. Commun.*, 2016, **52**, 12458–12461.

23 Z. Rong, R. Malik, P. Canepa, G. Sai Gautam, M. Liu, A. Jain, K. Persson and G. Ceder, *Chem. Mater.*, 2015, **27**, 6016–6021.

24 Z. Rong, P. Xiao, M. Liu, W. Huang, D. C. Hannah, W. Scullin, K. A. Persson and G. Ceder, *Chem. Commun.*, 2017, **53**, 7998–8001.

25 P. Canepa, S.-H. Bo, G. S. Gautam, B. Key, W. D. Richards, T. Shi, Y. Tian, Y. Wang, J. Li and G. Ceder, *Nat. Commun.*, 2017, **8**, 1759.

26 P. Canepa, G. Sai Gautam, D. C. Hannah, R. Malik, M. Liu, K. G. Gallagher, K. A. Persson and G. Ceder, *Chem. Rev.*, 2017, **117**, 4287–4341.

27 B. Morgan, DFT dataset, https://researchdata.bath.ac.uk/473/, (accessed April 30, 2018).

28 J. Ma, W. Li, B. J. Morgan, J. ŚwiĄtowska, R. Baddour-Hadjean, M. Body, C. Legein, O. J. Borkiewicz, S. Leclerc, H. Groult, F. Lantelme, C. Laberty-Robert and D. Dambournet, *Chem. Mater.*, 2018, **30**, 3078–3089.

29 A. Van der Ven, J. Bhattacharya and A. A. Belak, *Acc. Chem. Res.*, 2013, **46**, 1216–1225.

30 R. Kutner, *Phys. Lett. A*, 1981, **81**, 239–240.

31 W. Li, M. Fukunishi, B. J. Morgan, O. J. Borkiewicz, V. Pralong, A. Maignan, H. Groult, S. Komaba and D. Dambournet, *Inorg. Chem. Front.*, 2018, **5**, 1100–1106.